Tejedor, J, Macias-Guarasa, J, Martins, HF, Pastor-Graells, J, Martin-Lopez, S, Guillen, PC, De Pauw, G, De Smet, F, Postvoll, W, Ahlen, CH, Gonzalez-Herraez, M., 2018, "Real Field Deployment of a Smart Fiber-Optic Surveillance System for Pipeline Integrity Threat Detection: Architectural Issues and Blind Field Test Results", Journal of Lightwave Technology, 36 (4), pp. 1052 – 1062.

Available at http://dx.doi.org/10.1109/JLT.2017.2780126

Real Field Deployment of a Smart Fiber Optic Surveillance System for Pipeline Integrity Threat Detection: Architectural Issues and Blind Field Test Results

Javier Tejedor, Javier Macias-Guarasa, *Member, IEEE*, Hugo F. Martins, Juan Pastor-Graells, Sonia Martin-Lopez, Pedro Corredera, Guy De Pauw, Filip De Smet, Willy Postvoll, Carl H. Ahlen, and Miguel Gonzalez-Herraez

***Abstract*—This paper presents an on-line augmented surveillance system that aims to real time monitoring of activities along a pipeline. The system is deployed in a fully realistic scenario and exposed to real activities carried out in unknown places at unknown times within a given test time interval (so-called blind field tests). We describe the system architecture that includes specific modules to deal with the fact that continuous on-line monitoring needs to be carried out, while addressing the need of limiting the false alarms at reasonable rates. To the best or our knowledge, this is the first published work in which a pipeline integrity threat detection system is deployed in a realistic scenario (using a fiber optic along an active gas pipeline) and is thoroughly and objectively evaluated in realistic blind conditions. The system integrates two operation modes: The *machine+activity identification* mode identifies the machine that is carrying out a certain activity along the pipeline, and the *threat detection* mode directly identifies if the activity along the pipeline is a threat or not. The blind field tests are carried out in two different pipeline sections: The first section corresponds to the case where the sensor is close to the sensed area, while the second one places the sensed area about 35 km far from the sensor. Results of the machine+activity identification mode showed an average machine+activity classification rate of 46.6%. For the threat detection mode, 8 out of 10 threats were correctly detected, with only 1 false alarm appearing in a 55.5-hour sensed period.**

***Index Terms*—Distributed fiber sensing, Acoustic sensing, Vibration sensing, Pipeline integrity, phase-sensitive OTDR, Pattern recognition**

I. Introduction

Fiber optic distributed acoustic sensing (DAS) with phase-sensitive optical time-domain reflectometer (ϕ-OTDR) technology has been shown good performance for long perimeter monitorization aiming to detect intruders on the ground [1]–[5] or vibration in general [6]–[14].

Current pipeline integrity prevention systems combine DAS technology with a pattern recognition system (PRS) for continuous monitoring of potential threats to the pipeline integrity [15]–[22].

However, most of the works that employ DAS+PRS have shown significant issues with respect to the pattern classification design and evaluation, as presented in [23]. The main problems are related to the fact that no real classification is conducted nor results are given (e.g., [15], [16], [24]); not enough details on the system description or the experimental procedure are provided (e.g., [4], [16]–[18], [20]); the data generation process is far from being generated in a realistic field environment (e.g., [2], [10], [18], [24]), or this is even simulated (e.g., [7], [9], [10], [18], [25]–[29]).

Some recent works present significant improvements over those previously reported, by adopting more realistic recording environments (e.g., [17], [19]–[21], [30]), and more rigorous experimental procedures (e.g., [19], [20], [30]). However, there are still some issues related to the use of a single measurement position [19], [21], which implies a bias to recognize the position instead of the real event (whose effect was discussed in [22]), or the reduced number of the testing signals, with no additional details regarding the actual recording durations.

There are also companies that describe solutions for pipeline surveillance monitoring [16], although they do not usually provide enough details on their strategies, nor objective data for a proper assessment of their contribution.

The only exceptions that, to the best of our knowledge, aim to real field deployment of a DAS+PRS for pipeline integrity surveillance are found in [17] and [22], [23], [31], [32], but [17] does not provide enough details in its experimental procedure.

To assess the validity of a DAS+PRS that continuously monitors a long pipeline searching for potential threats and aims to real field deployment, a thorough experimental and validation procedure must be designed. This implies an approach that considers two experimental evaluation scenarios:

- An extensive off-line evaluation (that must employ recordings on realistic field data), which allows for an intensive experimental work to decide on the system design strategies and tuning.
- An (as much as possible) extensive on-line evaluation that should be based on tests carried out in real field scenarios, in unknown times, and unknown locations (so-called *blind field tests*). These blind field tests consist

J. Tejedor is with Fundación Universitaria San Pablo CEU.
H.F. Martins is with FOCUS S.L., Spain.
P. Corredera is with Instituto de Optica, CSIC, Spain.
G. De Paw is with Fluxys Belgium S.A.
F. De Smet is with Fluxys Belgium S.A.
W. Postvoll is with Gassco AS.
C. H. Ahlen is with Statoil AS.
J. Macias-Guarasa, J. Pastor-Graells, S. Martin-Lopez, and M. Gonzalez-Herraez are with the Department of Electronics, University of Alcalá, Spain.

in carrying out some activities at certain locations along the surveillance area at certain times within a given time interval (spanning from a few hours to days).

Regarding the extensive off-line evaluation scenario, in [22] we presented the first published report on a pipeline integrity threat detection system that employs DAS+PRS technology, was evaluated on realistic field data, and whose results are based on a rigorous experimental setup and an objective evaluation procedure with standard and clearly defined metrics. This work was further refined in [23], with an improved pattern recognition strategy that led to significant performance gains.

Regarding the on-line evaluation, we presented in [32] the first report on blind field tests of a pipeline integrity threat detection system, which addressed the experimental and validation procedure issues with respect to real field deployment. These field tests were carried out in realistic scenarios that comprised different locations and soil conditions, and were managed by Fluxys Belgium S.A., which was also responsible for hiring the corresponding machinery and equipment to carry out the required activities.

The pipeline integrity surveillance system consists in a combination of hardware and software modules. The hardware side refers to the DAS system used to record the data and the software side refers to the pattern classification system that classifies the acoustic data acquired by the sensing system. Two different operation modes were set up in the pipeline integrity surveillance system: machine+activity identification mode, where both the machine and the activity are identified, and threat detection mode, where just the occurrence of a threat in the pipeline must be detected.

With respect to our previous work [32], this paper (1) presents an augmented system with a new design that completes the baseline architecture with the required modules and strategies to face the specific conditions of a blind field test task operating in a fully real system deployment, and (2) provides additional system results and a deeper result analysis.

Therefore, it can be said that, to the best or our knowledge, this is the first published work in which a pipeline integrity threat detection system is deployed in a realistic scenario (using a fiber optic along an active gas pipeline) and is thoroughly and objectively evaluated in realistic blind conditions.

The rest of the paper is organized as follows: Section II presents the pipeline integrity threat detection system. The experimental procedure is presented in Section III. The results and discussion are presented in Section IV, and Section V concludes this paper.

II. Pipeline Integrity Threat Detection System

The pipeline integrity threat detection system integrates different modules, as shown in Figure 1, being an evolution of the architecture described in [22] to consider the modifications required for field operation in the blind field test task (new modules are shown in bold italic font). These modules are explained in more detail next.

A. Distributed Acoustic Sensing System

The DAS system is a commercially available ϕ-OTDR-based sensor named FINDAS, manufactured and distributed by FOCUS S.L. [33]. A detailed description of the sensing principle and experimental setup used in the FINDAS sensor was presented in [27].

The FINDAS has an (optical) spatial resolution of 5 meters (readout resolution of one meter) and a typical sensing range of up to 45 kms, using standard single-mode fiber (SMF). The fiber scanning rate (pulse repetition rate) was of 1085 Hz, so that the acoustic sampling frequency is also $f_s = 1085$ Hz. The optical sampling rate used in the data acquisition system was of 100 MHz.

B. Threat Location Preselection

Due to the fact that the system is running continuously and that the sensed positions are in the order of thousands, it is not possible to record all the acoustic traces along the fiber (due to restrictions in processing times, storage, and/or communication throughput). Therefore, a preselection of the positions which will actually be evaluated in search of possible threats must be carried out. In this way, only preselected traces will be processed in the PRS side.

This selection may use a threshold-based strategy from the energy measurements of the vibrations along the fiber, as presented in [32]: When the energy of the vibrations occurring in a given position of the fiber is above a predefined threshold, an acoustic trace is recorded to indicate a possible suspicious activity occurring at that point, and the trace is further processed by the PRS.

The simultaneous detection of multiple activities at different positions is also possible, by setting a different threshold for each position. The information of how this energy threshold profile was estimated is given in Section III-C.

C. Feature Extraction + Normalization

FINDAS is configured to record 20-second length acoustic traces that will be sent to the feature extraction module, which adopts a standard overlapped frame analysis approach. Signal frames to analyze are 1-second long, and the overlap is set to 95% to achieve a smoother change of the feature vectors. The Fast Fourier Transform (FFT) size was set to 8192 points. All these parameters were chosen as the optimal ones in an extensive experimentation effort carried out in our previous work [22].

In our current implementation, the feature extraction module calculates a feature vector composed of the energy values corresponding to 100 frequency bands for a 100 Hz bandwidth, using a sensitivity-based normalization (see [22] for more details). Again, this parameter configuration was selected as it achieved the best results in our previous work [22].

D. Pattern Classification

The pattern classification module employs a Gaussian Mixture Model (GMM)-based approach to classify each feature vector into the most likely class (machine+activity pair in the machine+activity identification mode, and threat/non-threat in the threat detection mode). This employs the a posteriori maximum probability criterion to assign the given feature vector the class with the highest probability given by the corresponding GMM (see [22] for more details).

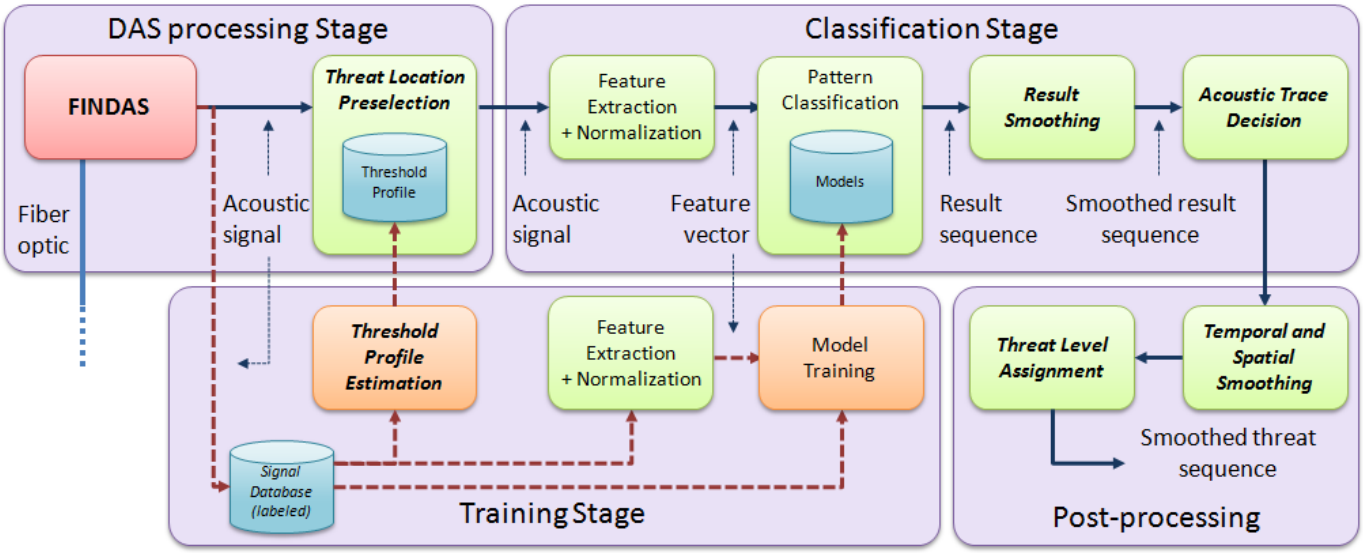

Fig. 1. Architecture of the pipeline integrity threat detection system. Modules in bold italics are new additions to face the real field deployment and the blind field test task (as compared with the architecture shown in [22]).

E. Result Smoothing

Given the 20-second length acoustic traces generated by the FINDAS, the frame length of 1 second and the frame overlap of 950 ms, and the fact that the classification process outputs one classification per acoustic frame, there are 415 frames (and therefore 415 classifications) in each acoustic trace.

With this setup (no matter the large frame overlap), it is highly probable that consecutive frames will be assigned different decisions (due to the characteristics of the GMM-based PRS, 'outlier' signal behavior, or artificial effects present when the signal was recorded), so that we decided to apply a process to smooth the actual result sequence output by the classifier.

Several strategies can be employed for the smoothing process, which are presented next.

1) Raw Smoothing: This strategy is based on substituting each frame decision (given by the corresponding class label) taking into account the decisions of the surrounding frames given a certain temporal window.

More specifically, given a temporal window of a fixed duration, this strategy replaces the recognition class given to every frame that falls in the current window by the majority class found in this window.

As an example, given the recognition sequence '14211121111', which corresponds to a certain temporal window of duration equals to 11 frames, this raw smoothing strategy will produce the new recognition sequence '11111111111', since the label '1' is the majority class in the given window.

2) Sliding Window Smoothing: The sliding window smoothing strategy bases on the previous one (raw smoothing). In this case, only the central frame (instead of all the frames) of a certain window is replaced by the majority class in the current window. A slide window of 1 frame is applied for this strategy.

As an example, given the recognition sequence '14211122222' in a certain temporal smoothing window of duration equals to 11 frames, the sixth frame (i.e., the one in the middle) is replaced by the majority class in this window to produce the new recognition sequence '14211222222'.

For frames that are at the beginning and end of an acoustic trace, the temporal window size is set to a value so that all the frames are *smoothed*.

3) Confusion Matrix-based Smoothing: The raw and sliding window smoothing strategies are based on the surrounding frame decisions to re-assign the decision for a given frame, without any additional information on the expected accuracy of the classification process. The rationale for the confusion matrix-based smoothing relies in the fact that performance improvements could be obtained by taking into account the possible classification errors that may exist between two given classes.

To add the information related to the classification errors, a confusion matrix that stores the probability of confusing every class with every other needs to be calculated.

The procedure used to build this confusion matrix is given in Section III.

The smoothing process consists in a dynamic programming algorithm [34] that calculates a distance of the given frame decision segment to each of the classes from the confusion matrix. The distance is computed from the minimum amount of substitutions, insertions, and deletions that are necessary to transform the input decision frames to the actual frames of each class. The algorithm next assigns all the frames of the given window the class whose distance to the input decision frames is the lowest given the confusion matrix.

In all the smoothing strategies, temporal window lengths of 1, 5, 10, and 20 seconds were evaluated.

F. Acoustic Trace Decision

After the result smoothing, the system still has 415 frame decisions for a certain acoustic trace. Therefore, to classify

this as a machine+activity pair or threat/non-threat depending on the system mode, a method to combine the 415 individual frame classifications into a single class is needed. We have adopted a majority voting scheme, where the acoustic trace is assigned the class for which more frames are classified.

G. Temporal and Spatial Smoothing

One of the main problems to face in real field deployment of a DAS+PRS is keeping false alarms under reasonable values. The fact that the DAS+PRS is run continuously, the characteristics of the sensing mechanism, and that the vibrations will affect a given length of the optical fiber being sensed, there may be possible threats that:

- Could be detected, but their duration across a given fiber length is not long enough to be considered as potential threats.
- Could be detected as independent of others, but:
  - They may be geographically close enough to each other, so that they should be considered as corresponding to the same physical event.
  - They may be temporally close enough to each other, so that they should be considered as corresponding to the same temporal event.

Specific strategies must be designed to alleviate this problem, for which our proposal contemplates two directions:

- Require the detected activities to have a minimum duration along nearby positions to be actually considered as such. Otherwise, they would be considered *spurious* events.
- Consider the detected activities to be corresponding to the same one, if they are separated less than a given distance within a given time interval.

H. Threat Level Assignment

In the threat detection mode of the pipeline integrity threat detection system, a method to evaluate the potential risk level of a detected threat was added to the system in order to provide additional details on the threat characteristics to the system operators (in a real world deployment). To do so, we based on the energy of the acoustic signal corresponding to the threat, so that four different risk levels were considered [1]. In a real world deployment, this could be encoded in a color scale, for example: light blue (which represents the lowest energy threats), light green, orange, and red (which represents the highest energy threats (and hence the most critical threats)) levels. The energy ranges that comprise each risk level are decided dividing the energy range of the detected threats in homogeneous segments.

III. Experimental Procedure

A. Blind Field Tests

Two different rounds of blind field tests were carried out to evaluate the system performance. Table I presents information on the distance from the sensor to the sensed area, the sensed location span (i.e., the length of the sensed area where the tests were carried out), the recording dates and times, and the total number of activities and threat activities carried out for each blind field test.

The first round of tests (SEC1) was carried out in a location near the DAS system, which favors a better Signal-to-Noise Ratio (SNR) in the signal acquisition process. On the other hand, the second round of tests (SEC2) was carried out in a zone that spreads from 31.5 kilometers to 36.5 kilometers far from the sensor, for which significant signal degradation should be observed. Therefore, better performance is expected in SEC1 as compared to SEC2.

B. Database Generation and Labeling

Database generation consists in obtaining the data that will be used for training, validation, and testing the system. The training data will be used for system training, the validation data will be used for system configuration and parameter tuning, and the testing data will be used to evaluate the system performance. In all cases, an accurate labeling (in terms of time stamps and activity being carried out) is fundamental for system training, system validation, and to generate the *ground truth* information that will be used in the system performance evaluation (by comparing it with the system results).

The database comprises the signal recordings carried out along a 45-kilometer length active gas pipeline operated by Fluxys Belgium S.A. Table II presents relevant information of the database acquisition related to the locations, environmental conditions, and recording period.

Training data comprise 22.5 hours of acoustic signals corresponding to different machines and activities that are potentially identifiable (e.g., excavators that are moving/hitting/scrapping/removing trees, drilling machines, pneumatic hammer, plate compactor, hammer, people walking, etc.). These training data were used to generate 45 models, each of which represents a certain machine+activity pair for the machine+activity identification mode of the system, and were next labeled with threat/non-threat labels to build the 2 models (that represent the *threat*/*non-threat* classes) employed in the threat detection mode of the system.

Validation data comprise a subset of 10 hours of the training data (those recorded in all the locations in Table II except LOC1) and correspond to 8 machine+activity pairs, which were employed for system configuration and tuning. More information of these validation data can be found in [22].

Table III shows the machine+activity pairs recorded along with their duration and the corresponding threat/non-threat labels for the training and validation data.

The test data comprise the continuous recordings that were done during the two rounds of blind field tests carried out in three different days. Table IV shows the machine+activity pairs recorded along with the timestamps, the location, and the corresponding threat/non-threat labels for the test data. Of course, the *ground truth* information was not known when the system was operating in field, and this was only used in the performance evaluation process. SEC1 tests ran for around 8

[1]These categories were agreed with the GERG members in the PIT-STOP project.

TABLE I
GENERAL INFORMATION REGARDING TO THE BLIND FIELD TESTS. 'KMS' STANDS FOR KILOMETERS.

Blind field test ID	Distance from the sensor (kms)	Recording day/s	Recording time	Number of activities	Number of threats
SEC1	0.3	1 day	8 hours	14	6
SEC2	31.5-36.5	2 days	2×24 hours	13	4

TABLE II
ENVIRONMENTAL, DATE, AND DISTANCE DETAILS ON LOCATIONS WHERE TRAINING AND VALIDATION DATA RECORDINGS TOOK PLACE. 'KMS' STANDS FOR KILOMETERS.

	LOC1	LOC2	LOC3	LOC4	LOC5	LOC6	LOC7
Distance from sensor (kms)	0.20	22.24	22.49	23.75	27.43	27.53	34.27
Soil condition	Concrete, wooden & grass in forest	Grass & clay in agricultural field	Grass in agricultural field	Concrete, grass & clay. Next to public street & private house	Wet clay in agricultural field	Clay in agricultural field	Grass in forest
Weather condition	Sunny/cloudy/rainy	Sunny/cloudy	Sunny	Sunny	Rainy	Cloudy	Sunny
Recording day/s	24-27 March 2015	15 October 2014	15 October 2014	14 October 2014	16 October 2014	16 October 2014	17 October 2014

TABLE III
TRAINING+VALIDATION DATA: MACHINE+ACTIVITY PAIRS WITH THEIR CORRESPONDING DURATION IN MINUTES AND THREAT/NON-THREAT LABELS (BETWEEN BRACKETS). ALL THE MACHINE+ACTIVITY PAIRS WERE EMPLOYED FOR SYSTEM TRAINING. THE MACHINE+ACTIVITY PAIRS EMPLOYED FOR VALIDATION ARE MARKED WITH '*'. ALL THE PAIRS EXCEPT THOSE MARKED WITH '*' WERE RECORDED IN LOC1, AND THE PAIRS MARKED WITH '*' WERE RECORDED IN THE REST OF THE LOCATIONS. '(T/NT)' STANDS FOR (THREAT/NON-THREAT). 'BIG EXCAVATOR' IS A 5 TON KUBOTA. 'MIDDLE EXCAVATOR' IS A 4 TON KUBOTA. 'SMALL EXCAVATOR' IS A 1.5 TON KUBOTA.

Machine+activity pair (duration) (T/NT)	Machine+activity pair (duration) (T/NT)	Machine+activity pair (duration) (T/NT)
Big excavator +unloading (4.3) (T)	Rocket drilling +small hitting (23.3) (T)	Hammer +big hitting (5.3) (T)
Big excavator +install wooden plates (47.3) (NT)	Rocket drilling +big drilling (31.0) (T)	Big excavator +metal sheet damming soil (20.7) (T)
Big excavator +movement (36.0) (NT)	Rocket drilling +big scrapping (12.7) (T)	Big excavator +metal sheet damming touching dummy (8.7) (T)
Big excavator +removing trees (11.7) (T)	Rocket drilling +big hitting (28.0) (T)	Big excavator +metal sheet damming hitting dummy (10.0) (T)
Big excavator +digging pit (30.3) (T)	Directional drilling +unloading (2.0) (NT)	People +walking (15.3) (NT)
Big excavator +install dummy (5.7) (NT)	Directional drilling +movement (10.3) (NT)	People +knocking fence door (7.0) (T)
Big excavator +insert sand in compact soil (20.0) (NT)	Directional drilling +small scrapping (27.3) (T)	Plate compactor +calibration (21.3) (NT)
Big excavator +install concrete plate (1.0) (NT)	Directional drilling +big drilling (14.0) (T)	Big excavator +movement (1315.3) * (NT)
Big excavator +scrapping dummy (16.0) (T)	Directional drilling +big scrapping (11.7) (T)	Big excavator +hitting (106) * (T)
Big excavator +knocking dummy (3.0) (T)	Directional drilling +small hitting (34.7) (T)	Big excavator +scrapping (324) * (T)
Directional drilling +preparations (10.3) (T)	Directional drilling +small drilling (87.7) (T)	Small excavator +movement (610) * (NT)
Middle excavator +movement (29.7) (NT)	Shelter pin +knocking (40.0) (T)	Small excavator +hitting (114) * (T)
Middle excavator +digging pit (30.3) (T)	Middle excavator +unloading (0.7) (NT)	Small excavator +scrapping (260) * (T)
Rocket drilling +small drilling (47.0) (T)	Middle excavator +hitting (22.0) (T)	Pneumatic hammer +working (388) * (NT)
Rocket drilling +small scrapping (21.0) (T)	Hammer +small hitting (5.3) (T)	Plate compactor +working (440) * (NT)

hours in the selected day, and SEC2 tests spread continuously during two consecutive days.

C. System Configuration

There are several parameters that are needed to be set along the different modules of the DAS and pipeline integrity threat detection systems.

First of all, the energy threshold profile that allows FINDAS to select which acoustic traces will be processed by the PRS had to be estimated. The energy threshold values were estimated for each single fiber location (as described in Section II-B). To do so, FINDAS was set to continuously record the energy profile of the fiber segment where the blind field tests were going to be performed. The energy profile recordings were done during 3 consecutive days for the SEC1

TABLE IV
TESTING DATA: MACHINE+ACTIVITY PAIRS WITH THEIR CORRESPONDING DURATION IN MINUTES AND THREAT/NON-THREAT LABELS (BETWEEN BRACKETS). SEC1 REFERS TO THE FIRST ROUND OF BLIND FIELD TEST LOCATION, AND SEC2 REFERS TO THE SECOND ONE. '(T/NT)' STANDS FOR (THREAT/NON-THREAT). 'BIG EXCAVATOR' IS AN 18 TON KUBOTA. 'MIDDLE EXCAVATOR' IS A 4 TON KUBOTA. 'SMALL EXCAVATOR' IS A 1.5 TON KUBOTA. 'DAMPLANKEN' IS A BIG EXCAVATOR.

Blind field test ID	Machine+activity pair (duration) (T/NT)	Machine+activity pair (duration) (T/NT)
SEC1	People+unloading rocket tools (20) (NT)	People+detect pipeline with hand shovels (20) (NT)
	Big excavator+movement (7) (NT)	People+unloading of excavator and tools (21) (NT)
	Big excavator+digging pit (5) (T)	Big excavator+hitting (1) (T)
	Rocket drilling+small drilling (24) (T)	Rocket drilling+big drilling (14) (T)
	Plate compactor+working (1) (NT)	Big excavator+filling pit (19) (NT)
	Prepare damplanken (21) (NT)	Damplanken+working (12) (T)
	Small excavator+movement (5) (NT)	Small excavator+digging and closing pit (8) (T)
SEC2	Middle excavator+movement (10) (NT)	Truck+movement (5) (NT)
	People+digging with shovels (11) (NT)	Middle excavator+digging pit (7) (T)
	Middle excavator+hitting (1) (T)	Drilling+preparations (6) (NT)
	Rocket drilling+small drilling (15) (T)	Rocket drilling+big drilling (17) (T)
	Small excavator+closing pit (9) (NT)	Small excavator+movement (2) (NT)
	Plate compactor+working and damming (10) (NT)	Drill compactor+drilling on soil and steel (6) (NT)
	Middle excavator and truck+movement (2) (NT)	

tests and 5 consecutive days for the SEC2 tests. From these recordings, the average energy was calculated for each fiber position, and this was established as the *background noise* level profile.

To establish the actual energy threshold profile, the energy range at the selected position must be taken into account, considering the background noise level, and also the expected energy levels for activities at the corresponding positions (that heavily depend on the distance to the interrogator). For example, in the SEC1 tests, which took place at an average of 300 meters far from the FINDAS, the threshold energy was set to 10 times the average background noise energy level measured for each fiber location point. For the SEC2 tests, which took place at an average of 34 kms far from the FINDAS, the threshold energy was simply set to the average noise energy level. These threshold energy values were selected by varying the multiplicative factor with respect to the average background noise energy level from 1 to 40 times in the corresponding location, and choosing the factor so that all the acoustic traces of the training data have an energy above the energy threshold (no testing data were used in the threshold estimation procedures).

Regarding the pattern classification module, a single-component GMM was trained for each class.[2]

In the confusion matrix-based smoothing (described in Section II-E3), the confusion matrix was built using a leave-one-out cross-validation (CV) approach from all the locations except LOC1 in Table II. To do so, four locations were used for system training, one location was used to build the confusion matrix, and the other location was used for system evaluation.

In the temporal and spatial smoothing module (see Section II-G), the acoustic traces corresponding to activities that spread less than 80 seconds along 40 meters were considered spurious. In the same way, consecutive threat decisions that are separated less than 80 seconds and 40 meters from the previous threat were grouped as corresponding to the same threat. These values were tuned on validation data across different time-space configurations. To do so, the time values were swept from 10 to 130 seconds, and the space values were swept from 0 to 60 meters. Again, no testing data were used in the parameter tuning procedures.

For the threat detection mode of the system, the class (threat or non-threat) with the highest probability (generated by the GMM-based pattern classification module) is selected as the corresponding to the evaluated acoustic trace, so that there is no need to establish a threshold value to compare with.

D. Evaluation Metrics

Classification accuracy has been the main metric to evaluate the system performance both for the machine+activity identification and threat detection modes. This is computed as the ratio between the number of correctly classified testing machines or activities, and the total number of evaluated activities. A machine+activity pair is considered to be correctly detected in case the machine or the activity output by the system coincides with that of the ground truth and is within the temporal limits of the activity ground-truth time span. In the same way, a threat is correctly detected in case the system generates a threat decision within the ground truth temporal limits.

Additionally, for the threat detection mode, the *Threat Detection Rate* (TDR), which corresponds to the percentage of threat testing activities that are classified as threat, usually referred to as *true positives*, and the *False Alarm Rate* (FAR), which corresponds to the percentage of non-threat testing activities that are classified as threats, usually referred to as *false positives*, were also calculated.

IV. EXPERIMENTAL RESULTS

A. Performance of the Result Smoothing Module

As described in Section II-E, three different strategies were examined to improve the system performance at frame level. However, during the blind field tests, one of these strategies must be chosen in the system pipeline.

[2]Training multi-dimensional GMMs was also tested, but the system performance was lower, probably due to data scarcity for certain machine+activity pairs.

Validation data were employed to select the optimal strategy. To do so, and since these data were recorded in 6 different locations (all except LOC1 in Table II), we applied a CV approach in a location basis (more details can be found in Section IV.D of [22]). This CV slightly varies depending on the smoothing strategy. For the raw smoothing and sliding window smoothing strategies, 5 locations were used for GMM training and the other location was employed as test to form 6 different folds. The different window sizes were examined for each fold, and the average performance from the results obtained in each fold and window size was computed. For the confusion matrix-based smoothing strategy, 4 locations were used for GMM training, one location was used to build the confusion matrix, and the other for testing. This derives in 30 folds. As in the other strategies, the average performance is obtained by averaging the performance for each fold.

The smoothing results are presented in Table V for the machine+activity identification and threat detection modes, compared with the ones obtained without smoothing. These results show that longer window sizes are better than shorter window sizes. Since more information (decisions of more frames) is considered for the decision, and all the frames that comprise an acoustic trace belong to a same activity, better performance is expected.

The best result is obtained by the raw smoothing strategy with the 20-second length window for almost all the metrics. For the machine+activity classification accuracy (**MAC accuracy** in Table V), the raw smoothing and sliding window smoothing strategies obtain similar performance, being the former slightly better than the latter. On the other hand, the confusion matrix-based smoothing strategy obtains the worst results, probably due to data scarcity issues.

For the threat classification accuracy (**TC accuracy** in Table V), the confusion matrix-based smoothing strategy obtains a slightly better overall performance. However, in this system mode, the TDR and the FAR are more adequate to decide which strategy is better, so that we can see that the raw smoothing strategy obtains better TDR. Since detecting as many threats as possible is crucial when building this kind of systems, we have selected the raw smoothing strategy with window size equals to 20 seconds for the real field deployment tests.

B. Time-Location Based Analysis

Preliminary analysis was carried out to get an initial idea on the feasibility of the pipeline integrity surveillance system for detecting suspicious activities in the surveillance zones corresponding to the two rounds of blind field tests. This analysis consists in a time-location sensed energy representation of the surveilled zone that aims to be monitored in each blind field test. Figure 2 shows the time-location energy representation for the SEC1 blind field tests, where the horizontal axis shows the time, and the vertical axis shows the distance at which a given energy value (in a thermal color scale from blue to red) was measured. We do not show the full time-location energy representation for the SEC2 blind field tests, as it was mostly *empty*, given that the test was only done during 4 hours of the day 2 of the tests. Instead, we show Figure 3, which is a zoomed in version of the time-location energy representation of the SEC2 blind field tests, centered in the time-location area where the test activities were carried out (around 34.4 km from the sensor and between 9:00 and 13:00 of the second recording day).

These figures show that all activities were detected by the FINDAS in both rounds of blind field tests, and they turned out to be at the correct times when the activities were being carried out. This means that the energy-based threshold estimation procedure was highly accurate. In the blind field test location near the FINDAS (Figure 2), the time-location energy representation reveals *clearer* information, due to the higher SNR in the data acquisition. In the case of the SEC2 test, where the sensed location is 34 kms far from the sensor, much lower energy values are reported, which derives in a much more difficult activity detection. However, the figure shows that the system was able to detect all the activities.

C. Blind Field Test System Results

After verifying that all the activities were correctly detected by the FINDAS, the system performance for the blind field tests in terms of quantitative rates regarding to the classification itself are presented in Table VI.

These results show that, as expected, SEC1 obtains better performance than SEC2, due to the favorable acoustic signal conditions. It can also be seen that almost all the threats are correctly detected, which suggests that the system is suitable for real field deployment.

With respect to the identification of the machine+activity pair, the performance drops. On the one hand, this is due to the very high number of classes involved in the system (45 in our case). Nevertheless, the average MAC accuracy is 46.6%, much higher than the pure chance rate (11% given that there are 10 different machines and 31 different activities), which is promising given the extreme difficulty of the task. This performance for the machine+activity classification task is comparable with the 54.92% presented in our previous study for offline tests described in [23], in which a much simpler experimental setup was used (4 different machines and 8 different activities, with a 12.5% pure chance rate).

On the other hand, a detailed analysis of the errors in the machine+activity identification mode reveals interesting findings: For SEC1, a performance loss of 26.7% is due to the fact that there was no trained model for the performed activity. The other 20% drop corresponds to machine+activity pairs that have been incorrectly classified by the system. For SEC2, a performance loss of 30.7% is again due to the unavailability of a trained model for the performed activity, being the other 30.7% performance drop due to actual classification errors. The reason why there are some activities carried out in the blind field tests that do not have a corresponding model trained, is that the GERG members wanted to evaluate what would be the system response in such cases (i.e., facing an unknown activity). The training and validation data sets (used for system training and building) were recorded before the blind field tests were carried out. Therefore, the non-previously trained activities used in the blind tests could

TABLE V
RESULTS OF THE DIFFERENT SMOOTHING STRATEGIES FOR MACHINE+ACTIVITY IDENTIFICATION AND THREAT DETECTION MODES WITH THE BEST RESULT IN BOLD FONT. 'MAC' STANDS FOR MACHINE+ACTIVITY CLASSIFICATION, 'TC' FOR THREAT CLASSIFICATION, 'TDR' FOR THREAT DETECTION RATE, AND 'FAR' FOR FALSE ALARM RATE.

Smoothing type	Window length (seconds)	MAC accuracy	TC accuracy	TDR	FAR
None	-	$45.2\% \pm 0.11\%$	$64.3\% \pm 0.11\%$	$80.7\% \pm 0.09\%$	$40.3\% \pm 0.11\%$
Raw	1	$50.6\% \pm 0.11\%$	$65.3\% \pm 0.11\%$	$84.5\% \pm 0.08\%$	$40.3\% \pm 0.11\%$
Raw	5	$56.9\% \pm 0.11\%$	$67.1\% \pm 0.11\%$	$88.9\% \pm 0.07\%$	$39.2\% \pm 0.11\%$
Raw	10	$59.6\% \pm 0.11\%$	$68.2\% \pm 0.11\%$	$91.0\% \pm 0.07\%$	$38.4\% \pm 0.11\%$
Raw	20	$\mathbf{61.9\% \pm 0.11\%}$	$\mathbf{69.2\% \pm 0.11\%}$	$\mathbf{92.0\% \pm 0.06\%}$	$\mathbf{37.5\% \pm 0.11\%}$
Sliding window	1	$50.4\% \pm 0.11\%$	$65.4\% \pm 0.11\%$	$84.4\% \pm 0.08\%$	$40.2\% \pm 0.11\%$
Sliding window	5	$56.8\% \pm 0.11\%$	$67.2\% \pm 0.11\%$	$88.9\% \pm 0.07\%$	$39.1\% \pm 0.11\%$
Sliding window	10	$59.1\% \pm 0.11\%$	$67.9\% \pm 0.11\%$	$90.5\% \pm 0.07\%$	$38.7\% \pm 0.11\%$
Sliding window	20	$61.3\% \pm 0.11\%$	$68.8\% \pm 0.11\%$	$91.3\% \pm 0.06\%$	$37.7\% \pm 0.11\%$
Confusion matrix	1	$49.9\% \pm 0.11\%$	$65.9\% \pm 0.11\%$	$83.2\% \pm 0.09\%$	$39.1\% \pm 0.11\%$
Confusion matrix	5	$55.4\% \pm 0.11\%$	$68.0\% \pm 0.11\%$	$87.2\% \pm 0.08\%$	$37.7\% \pm 0.11\%$
Confusion matrix	10	$57.7\% \pm 0.11\%$	$68.7\% \pm 0.10\%$	$89.1\% \pm 0.07\%$	$37.3\% \pm 0.11\%$
Confusion matrix	20	$59.6\% \pm 0.11\%$	$69.7\% \pm 0.10\%$	$90.4\% \pm 0.07\%$	$36.3\% \pm 0.11\%$

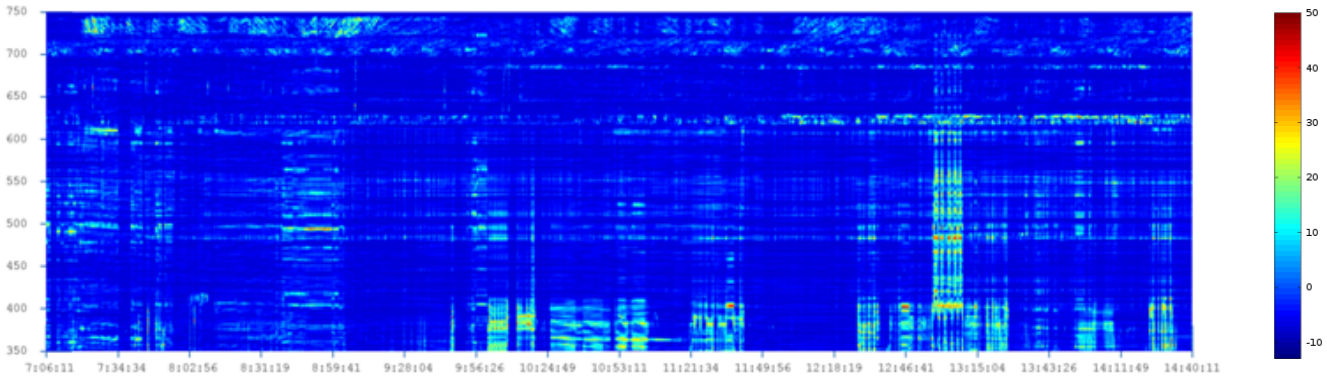

Fig. 2. Time-Location energy representation for the SEC1 blind field tests. x-axis is in format HH:MM:SS where HH denotes hours, MM denotes minutes, and SS denotes seconds. For clarity, when the hour only contains one digit, there is only one number representing HH. y-axis is given in meters, where the meter value grows with the distance to the FINDAS (i.e., 350 represents 350 meters far from the sensor). Colorbar scale is in dBs.

TABLE VI
BLIND FIELD TEST SYSTEM RESULTS. 'MAC' STANDS FOR MACHINE+ACTIVITY CLASSIFICATION, 'ACC.' FOR ACCURACY, 'TC' FOR THREAT CLASSIFICATION, 'TDR' FOR THREAT DETECTION RATE, AND 'FAR' FOR FALSE ALARM RATE.

Blind field test ID	MAC acc.	TC acc.	TDR	FAR
SEC1	53.3%	100.0%	100.0%	0.0%
SEC2	38.5%	76.9%	50.0%	25.0%
Average	46.6%	88.9%	80.0%	10.0%

not (and must not) be included in the system training. The activities for which there is no trained model were: People+unloading rocket tools, People+detect pipeline with hand shovels, People+unloading of excavator and tools, Big excavator+filling pit, Prepare damplanken, Small excavator+digging and closing pit, Truck+movement, People+digging with shovels, Drilling+preparations, Small excavator+closing pit, and Drill compactor+drilling on soil and steel. The performance drop observed for activities with unseen data in the training stage is obviously expected, and proves the need of addressing a data acquisition effort as wide as possible, as stated in [35].

In both SEC1 and SEC2 blind field tests, the classification errors come from different sources: (1) the machines carried out the activities during certain times that did not fulfill the temporal restriction in the temporal and spatial smooth module, (2) confusions due to similarity in activities such as hitting or scrapping (scrapping sometimes includes some hitting), and (3) overlapping of different activities in a single one. In addition, the different (unknown) testing locations along the pipeline imply different acoustic conditions (soil, weather, etc.) in the acquired acoustic traces, and this variability affects to a great extent the system performance, as was already discussed in our previous publications (c.f. Section IV.C of [22]). Our strategy partially alleviates the issue related to acoustic variability in unknown environments, by first obtaining training data from as many different locations, days, and times as possible (so that the acoustic models can learn and generalize such variability); then, by applying specific normalization approaches to the acoustic traces; and finally, by employing smoothing procedures to the obtained results.

Since this is an on-line system that continuously monitors potential threats for the pipeline, real time response is crucial. All the system modules except the *Pattern Classification* module have a computational cost that does not depend on the number of models. For the latter module, more models increase the response time as the acoustic trace has to be compared with all the trained models. Experiments were run

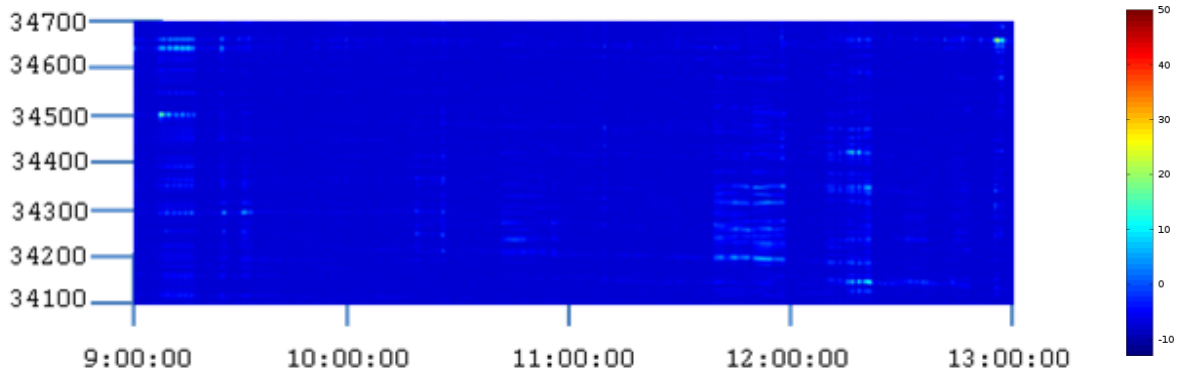

Fig. 3. Zoomed in version of the Time-Location energy representation of the SEC2 blind field tests, centered in the time-location area where the test activities were carried out (around 34.4 km from the sensor and between 9:00 and 13:00 of the second recording day). x-axis, y-axis, and colorbar are in the same format as in Figure 2.

on an Intel Quad Q9550 2.83GHz processor and 4GB RAM. Table VII shows the computational time of the system modules. It can be seen that the system is able to run on real-time, since the time response is less than a second in any mode. The table also shows that each model added to the system increases the computational time in 10 ms. This means that, after the 20-second length acoustic trace has been recorded by the FINDAS, the decision assigned to the suspicious acoustic trace is given in 0.69 seconds in the machine+activity identification mode, and 0.26 seconds in the threat detection mode.

The information about the threat level assignment discussed in Section II-H was not used in the system result evaluation (as we were only interested in assessing the threat detection accuracy). The threat level calculation is meant to be exploited in future research.

As a final comment, the blind field test evaluation procedures will face, in most cases, the problem of the statistical significance of the results. In cases such as the one described in this paper, the number of blind field tests that can be performed will be much lower than the tests conducted during the off-line database evaluation process. Therefore, the reported results in the off-line evaluation will have a higher statistical significance than those from the blind field tests. This must be taken into account to put the blind field test results in an adequate context, and also to drive the design of a broad enough blind field test campaign.

V. Conclusions and Future Work

We have presented an evolution of the systems presented in [22] and [32] that is able to continuously monitor potential threats to the pipeline integrity in real field blind conditions. On-line pipeline integrity monitorization systems have to resort to a series of blind field tests to clearly assess their performance when facing at real field deployment. For this, two different rounds of blind field tests were conducted in different days and locations, which convey different acoustic signal properties each. The blind field test locations are placed near the sensing system (300 meters far) and far the sensing system (35 kilometers far).

Results show good performance in terms of threat detection, since 8 out of 10 threats were correctly detected, and just 1 false alarm in 55.5 hours was generated. In terms of machine+activity classification, the average performance is 46.6%, which is still well above chance (11%, given the 10 potential machines and 31 potential activities the system is able to detect). Results also show degradation as long as the distance to the sensing system increases, both in terms of machine+activity classification and threat detection rates.

Future work should address the signal degradation issue when the distance to the sensor grows. In addition, other feature extraction techniques (e.g., those based on wavelet transforms that take advantage of time and frequency domains simultaneously) and pattern classification techniques (e.g., combination of GMM and neural networks) must also be examined.

Acknowledgments

Some authors were supported by funding from the European Research Council through Starting Grant UFINE (grant number #307441), Water JPI, the WaterWorks2014 Cofunded Call, the European Commission (Horizon 2020) through project H2020-MSCA-ITN-2016/722509 - FINESSE, the Spanish Ministry of Economy and Competivity, the Spanish "Plan Nacional de I+D+i" through projects TEC2013-45265-R, TEC2015-71127-C2-2-R, TIN2013-47630-C2-1-R, and TIN2016-75982-C2-1-R, and the regional program SINFOTONCM: S2013/MIT-2790 funded by the "Comunidad de Madrid". HFM acknowledges funding through the FP7 ITN ICONE program, grant number #608099 funded by the European Commission. JPG acknowledges funding from the Spanish Ministry of Economy and Competivity through an FPI contract. SML acknowledges funding from the Spanish Ministry of Science and Innovation through a "Ramón y Cajal" contract.

References

[1] K. N. Choi, J. C. Juarez, and H. F. Taylor, "Distributed fiber optic pressure/seismic sensor for low-cost monitoring of long perimeters," in *Proc. of SPIE*, 2003, pp. 134–141.

TABLE VII
COMPUTATIONAL TIME OF THE SYSTEM MODULES (IN MILLISECONDS). THE COLUMN 'REST OF MODULES' INCLUDES THE COMPUTATIONAL TIME OF THE 'RESULT SMOOTHING', 'ACOUSTIC TRACE DECISION', 'TEMPORAL AND SPATIAL SMOOTHING', AND 'THREAT LEVEL ASSIGNMENT' MODULES.

System mode	Feature Extraction + Normalization	Pattern Classification	Rest of Modules	Total
Machine+Activity identification	140	450 (45 models)	100	690
Threat detection	140	20 (2 models)	100	260

[2] J. C. Juarez, E. W. Maier, K. N. Choi, and H. F. Taylor, "Distributed fiber-optic intrusion sensor system," *Journal of Lightwave Technology*, vol. 23, no. 6, pp. 2081–2087, 2005.

[3] J. C. Juarez and H. F. Taylor, "Field test of a distributed fiber-optic intrusion sensor system for long perimeters," *Applied Optics*, vol. 46, no. 11, pp. 1968–1971, 2007.

[4] Y.-J. Rao, J. Luo, Z.-L. Ran, J.-F. Yue, X.-D. Luo, and Z. Zhou, "Long-distance fiber-optic ψ-OTDR intrusion sensing system," in *Proc. of SPIE*, vol. 7503, 2009, pp. 75 031O–1–75 031O–4.

[5] J. C. Juarez and H. F. Taylor, "Polarization discrimination in a phase-sensitive optical time-domain reflectometer intrusion-sensor system," *Optics Letters*, vol. 30, no. 24, pp. 3284–3286, 2005.

[6] P. Chao, Z. Hui, Y. Bin, Z. Zhu, and S. Xiahoan, "Distributed optical-fiber vibration sensing system based on differential detection of differential coherent-OTDR," in *Proc. of IEEE Sensors*, 2012, pp. 1–3.

[7] Z. G. Quin, L. Chen, and X. Y. Bao, "Wavelet denoising method for improving detection performance of distributed vibration sensor," *IEEE Photonics Technology Letters*, vol. 24, no. 7, pp. 542–544, 2012.

[8] Z. N. Wang, J. Li, M. Q. Fan, L. Zhang, F. Peng, H. Wu, J. J. Zeng, Y. Zhou, and Y. J. Rao, "Phase-sensitive optical time-domain reflectometry with Brillouin amplification," *Optics Letters*, vol. 39, no. 15, pp. 4313–4316, 2014.

[9] H. F. Martins, S. Martín-López, P. Corredera, M. L. Filograno, O. Frazão, and M. González-Herráez, "Phase-sensitive optical time domain reflectometer assisted by first-order Raman amplification for distributed vibration sensing over $>$ 100 km," *Journal of Lightwave Technology*, vol. 32, no. 8, pp. 1510–1518, 2014.

[10] F. Peng, H. Wu, X.-H. Jia, Y.-J. Rao, Z.-N. Wang, and Z.-P. Peng, "Ultra-long high-sensitivity ϕ-OTDR for high spatial resolution intrusion detection of pipelines," *Optics Express*, vol. 22, no. 11, pp. 13 804–13 810, 2014.

[11] J. Li, Z. Wang, L. Zhang, F. Peng, S. Xiao, H. Wu, and Y. Rao, "124km phase-sensitive OTDR with Brillouin amplification," in *Proc. of SPIE*, vol. 9157, 2014, pp. 91 575Z–1–91 575Z–4.

[12] Z. Wang, J. Zeng, J. Li, F. Peng, L. Zhang, Y. Zhou, H. Wu, and Y. Rao, "175km phase-sensitive OTDR with hybrid distributed amplification," in *Proc. of SPIE*, vol. 9157, 2014, pp. 9157D5–1–9157D5–4.

[13] Z. Pan, Z. Wang, Q. Ye, H. Cai, R. Qu, and Z. Fang, "High sampling rate multi-pulse phase-sensitive OTDR employing frequency division multiplexing," in *Proc. of SPIE*, vol. 9157, 2014, pp. 91 576X–1–91 576X–4.

[14] Y. Shi, H. Feng, and Z. Zeng, "A long distance phase-sensitive optical time domain reflectometer with simple structure and high locating accuracy," *Sensors*, vol. 15, no. 9, pp. 21 957–21 970, 2015.

[15] H. Zhu, C. Pan, and X. Sun, "Vibration pattern recognition and classification in OTDR based distributed optical-fiber vibration sensing system," in *Proc. of SPIE*, vol. 9062, 2014, pp. 906 205–1–906 205–6.

[16] C. Conway and M. Mondanos, "An introduction to fibre optic intelligent distributed acoustic sensing (iDAS) technology for power industry applications," in *Proc. of International Conference on Insulated Power Cables*, vol. A3.4, 2015, pp. 1–6.

[17] H. Wu, Z. Wang, F. Peng, Z. Peng, X. Li, Y. Wu, and Y. Rao, "Field test of a fully distributed fiber optic intrusion detection system for long-distance security monitoring of national borderline," in *Proc. of SPIE*, vol. 91579, 2014, pp. 915 790–1–915 790–4.

[18] H. Wu, X. Li, Z. Peng, and Y. Rao, "A novel intrusion signal processing method for phase-sensitive optical time-domain reflectometry (ϕ-OTDR)," in *Proc. of SPIE*, vol. 9157, 2014, pp. 9157O–1–9157O–4.

[19] C. Cao, X. Y. Fan, Q. W. Liu, and Z. Y. He, "Practical pattern recognition system for distributed optical fiber intrusion monitoring system based on phase-sensitive coherent OTDR," in *Proc. of Asia Communications and Photonics Conference*, 2015, pp. 145:1–145:3.

[20] Q. Sun, H. Feng, X. Yan, and Z. Zeng, "Recognition of a phase-sensitivity OTDR sensing system based on morphologic feature extraction," *Sensors*, vol. 15, pp. 15 179–15 197, 2015.

[21] H. Wu, S. Xiao, X. Li, Z. Wang, J. Xu, and Y. Rao, "Separation and determination of the disturbing signals in phase-sensitive optical time domain reflectometry (ϕ-OTDR)," *Journal of Lightwave Technology*, vol. 33, no. 15, pp. 3156–3162, 2015.

[22] J. Tejedor, H. F. Martins, D. Piote, J. Macias-Guarasa, J. Pastor-Graells, S. Martin-Lopez, P. Corredera, F. D. Smet, W. Postvoll, and M. Gonzalez-Herraez, "Towards prevention of pipeline integrity threats using a smart fiber optic surveillance system," *Journal of Lightwave Technology*, vol. 34, no. 19, pp. 4445–4453, 2016.

[23] J. Tejedor, J. Macias-Guarasa, H. Martins, D. Piote, J. Pastor-Graells, S. Martin-Lopez, P. Corredera, and M. Gonzalez-Herraez, "A novel fiber optic based surveillance system for prevention of pipeline integrity threats," *Sensors*, vol. 17, no. 2, pp. E355:1–E355:19, 2017.

[24] C. Madsen, T. Baea, and T. Snider, "Intruder signature analysis from a phase-sensitive distributed fiber-optic perimeter sensor," in *Proc. of SPIE*, vol. 6770, 2007, pp. 67 700K–1–67 700K–8.

[25] Z. G. Quin, L. Chen, and X. Y. Bao, "Continuous wavelet transform for nonstationary vibration detection with phase-OTDR," *Optics Express*, vol. 20, no. 18, pp. 20 459–20 465, 2012.

[26] T. Zhu, X. Xiao, Q. He, and D. Diao, "Enhancement of SNR and spatial resolution in ψ-OTDR system by using two-dimensional edge detection method," *Journal of Lightwave Technology*, vol. 31, no. 17, pp. 2851–2856, 2013.

[27] H. F. Martins, S. Martín-López, P. Corredera, M. L. Filograno, O. Frazão, and M. González-Herráez, "Coherent noise reduction in high visibility phase sensitive optical time domain reflectometer for distributed sensing of ultrasonic waves," *Journal of Lightwave Technology*, vol. 31, no. 23, pp. 3631–3637, 2013.

[28] Z. Wang, J. Zeng, J. Li, M. Fan, H. Wu, F. Peng, L. Zhang, Y. Zhou, and Y. Rao, "Ultra-long phase-sensitive OTDR with hybrid distributed amplification," *Optics Letters*, vol. 39, no. 20, pp. 5866–5869, 2014.

[29] H. F. Martins, S. Martin-Lopez, P. Corredera, J. D. Ania-Castañon, O. Frazão, and M. Gonzalez-Herraez, "Distributed vibration sensing over 125 km with enhanced SNR using ϕ-OTDR over a URFL cavity," *Journal of Lightwave Technology*, vol. 33, no. 12, pp. 2628–2632, 2015.

[30] A. Papp, C. Wiesmeyr, M. Litzenberger, H. Garn, and W. Kropatsch, "A real-time algorithm for train position monitoring using optical time-domain reflectometry," in *Proc. of Intelligent Rail Transportation*, 2016, pp. 1–5.

[31] H. Martins, D. Piote, J. Tejedor, J. Macias, J. Pastor, S. Martin, P. Corredera, F. D. Smet, W. Postvoll, C. Ahlen, and M. Gonzalez, "Early detection of Pipeline Integrity Threats using a SmarT fiber-OPtic surveillance system: The PIT-STOP project," in *Proc. of International Conference on Optical Fibre Sensors*, 2015, pp. 96 347X:1–96 347X:4.

[32] H. Martins, D. Piote, J. Tejedor, J. Macias, J. Pastor, S. Martin, P. Corredera, F. D. Smet, W. Postvoll, C. Ahlen, and M. Gonzalez, "Towards detection of Pipeline Integrity Threats using a SmarT fiber-OPtic surveillance system: PIT-STOP project blind field test results," in *Proc. of International Conference on Optical Fibre Sensors*, 2017, pp. 103 231K:4–103 231K:4.

[33] FOCUS. S.L., "FIber Network Distributed Acoustic Sensor (FINDAS)," 2015, http://www.focustech.eu/FINDAS-MR-datasheet.pdf, Last access September 2016.

[34] L. Fissore, P. Laface, G. Micca, and R. Pieraccini, "Lexical access to large vocabularies for speech recognition," *IEEE Transactions on Acoustics, Speech, and Signal Processing*, vol. 37, no. 8, pp. 1197–1213, 1989.

[35] J. Tejedor, J. Macias-Guarasa, H. F. Martins, J. Pastor-Graells, P. Corredera, and S. Martin-Lopez, "Machine learning methods for pipeline surveillance systems based on distributed acoustic sensing: A review," *Applied Sciences*, vol. 7, no. 8, pp. 841:1–841:26, 2017.